Tuning the negative thermal expansion behavior of the metal–organic framework Cu_3BTC_2 by retrofitting

Christian Schneider, David Bodesheim,
Michael G. Ehrenreich, Valentina Crocellà, János Mink,
Roland A. Fischer, Keith T. Butler and Gregor Kieslich

Published version information

Citation: C Schneider et al. "Tuning the negative thermal expansion behavior of the metal-organic framework Cu3BTC2 by retrofitting." Journal of the American Chemical Society, vol. 141, no. 26 (2019): 10504-10509.

DOI: 10.1021/jacs.9b04755

Tuning the Negative Thermal Expansion Behavior of the Metal-Organic Framework Cu_3BTC_2 by Retrofitting

Christian Schneider,[a] David Bodesheim,[a] Michael G. Ehrenreich,[a] Valentina Crocellà,[b] János Mink,[c,d] Roland A. Fischer,[a] Keith T. Butler,[e] Gregor Kieslich*[a]

[a] Department of Chemistry, Technical University of Munich, Lichtenbergstrasse 4, D-85748 Garching, Germany.

[b] Department of Chemistry, NIS and INSTM Centre of Reference, University of Turin, Via Quarello 15, I-10135 Torino, Italy.

[c] Institute of Materials and Environmental Chemistry, Research Center of Natural Sciences, Hungarian Academy of Sciences, H-1519 Budapest, Hungary.

[d] Research Institute for Biomolecular and Chemical Engineering, University of Pannonia, H-8200 Veszprém, Hungary.

[e] Scientific Computing Department, Rutherford Appleton Laboratory, Harwell Campus, Didcot OX11 0QX, United Kingdom.

Metal-organic frameworks, negative thermal expansion, retrofitting, lattice dynamics

ABSTRACT: The modular building principle of metal-organic frameworks (MOFs) presents an excellent platform to explore and establish structure-property relations that tie microscopic to macroscopic properties. Negative thermal expansion (NTE) is a common phenomenon in MOFs and is often ascribed to collective motions that can move through the structure at sufficiently low energies. Here we show that the introduction of additional linkages in a parent framework – retrofitting – is an effective approach to access lattice dynamics experimentally, in turn providing researchers with a tool to alter the NTE behavior in MOFs. By introducing TCNQ (7,7,8,8-tetracyanoquinodimethane) into the prototypical MOF Cu_3BTC_2 (BTC = 1,3,5-benzenetricarboxylate; HKUST-1), NTE can be tuned between α_V = -15.3·10^{-6} K^{-1} (Cu_3BTC_2) and α_V = -8.4·10^{-6} K^{-1} (1.0TCNQ@Cu_3BTC_2). We ascribe this phenomenon to a general stiffening of the framework as a function of TCNQ loading, which is confirmed by computational modelling and far infrared spectroscopy. Our findings imply that retrofitting is generally applicable to MOFs with open metal sites, opening yet another way to fine-tune properties in this versatile class of materials.

Among the different phenomena in materials science and solid-state chemistry, it is the existence of counterintuitive materials properties that challenge our understanding of how to describe materials on a microscopic level. Properties such as negative thermal expansion (NTE),[1-3] negative linear compressibility (NLC),[4-6] or negative Poisson's ratio (NPR),[7-9] tie the macroscopic world with the microscopic world, helping us continuously to sharpen our perception of how to see and understand certain phenomena in materials. Sometimes seen as scientific curiosities, such effects can indeed have practical relevance. For instance, the thermal expansion (TE) behavior of a material is a crucial parameter in areas such as construction chemistry, dental care or electrical engineering, where the fabrication, processing and materials durability as a function of temperature variations plays a critical role. An important example is the fabrication of optical components, such as mirrors used in big telescopes, where materials with zero thermal expansion coefficients around the typical working temperature can ensure high-precision measurements.

Focusing on the thermal expansion behavior of a material, we can distinguish between materials that show positive thermal expansion (PTE, $\alpha_V > 0$), zero thermal expansion (ZTE, $\alpha_V \sim 0$) and negative thermal expansion (NTE, $\alpha_V < 0$), with α_V being the volumetric thermal expansion coefficient:

$$\alpha_V = \frac{1}{V}\frac{dV}{dT} \qquad \text{(eq. 1)}$$

where V is the volume of the unit cell and dV/dT the change of volume as a function of temperature. Whilst the majority of investigated materials exhibit PTE, NTE has been discovered in a number of material classes such as metal oxides,[10-11] metal cyanides,[12-13] and zeolites.[14-15] Recent research studies in this area focus on understanding the microscopic mechanism behind NTE in emerging materials, with the tunability of α_V being arguably one of the biggest challenges for experimentalists. It has been shown that α_V depends on various parameters that can be accessed experimentally. For instance, the redox intercalation of Li^+ ions into ScF_3 is an effective method to control thermal expansion behavior from NTE to PTE. [16] Similarly, guest-dependent thermal expansion has been observed for various Prussian Blue analogues and related materials such as $ZnPt(CN)_6$, $Fe_3[Co(CN)_6]_2$ and $Co[(Fe(CN)_5NO]$ where a complex relation exists between adsorbed H_2O or CO_2 molecules and α_V. Fundamentally, NTE in materials originates from either electronic or magnetic coupling phenomena or low energy phonons. In the latter case, collective motions are responsible for the on average shortened distances between respective building blocks.[1-2] An elegant concept that has proved to be useful to understand NTE in various materials are rigid unit modes (RUMs). Initially developed to explain displacive phase transitions in silicates and

related materials,[2] the RUM model provides a rather intuitive model how lattice dynamics can be coupled to NTE.

Metal-organic frameworks (MOFs) are one class of materials in which phonon-mediated NTE behavior is often observed. MOFs are coordination polymers constructed from metal-nodes that are interconnected by polydentate ligands to form (porous) 2D or 3D networks.[17-18] Interestingly, their building block principle as embodied in the reticular chemistry approach inherently reflects the RUM concept. In combination with the void pore space, it is easy to envision that only little energy is required for the excitation of (correlated) vibrations such as linker bending motions.[19] Examples include the iconic MOF-5 and Cu_3BTC_2 with thermal expansion coefficients of α_V = -39.3·10^{-6} K^{-1} and α_V = -12.3·10^{-6} K^{-1}, respectively.[20-21] MOF-5 is one of the better-investigated MOFs as nicely summarized by Dove and Fang.[2] Experimental and computational studies show that RUMs and trampoline-like vibrations of the BDC linker have a significant contribution to the NTE in MOF-5.[20, 22-23] Moreover, lattice dynamics in MOF-5 can be accessed by adsorption of He or small organic molecules leading to increasing thermal expansion coefficients.[24-25] The highest NTE of a MOF to date was reported for UiO-66(Hf), (α_V = -97·10^{-6} K^{-1}).[26] Importantly, the high degree of synthetic versatility of MOFs offers a great playground to tune the macroscopic response of MOFs to temperature and pressure.

In this context, the targeted incorporation of defects into a parent MOF has recently proved to be particularly exciting in the area of mechanical stability and catalysis.[25-29] When taking a relatively broad definition for a defect, *i.e.* defining a defect as feature that breaks periodicity, it is possible to distinguish between point defects such as missing linker or missing node defects, and the situation where guest molecules that are incorporated into the pores break periodicity, *i.e.* interstitial defects. Point defects in UiO-66(Hf) have recently been used to manipulate α_V, with a larger defect concentration leading to decrease in NTE behavior. It was speculated that a volume effect together with the presence of metal-node related symmetry-breaking phenomena is responsible for this observation.[26] Likewise, point defects have been used to alter the mechanical response of UiO-66(Zr), where a complex relation between bulk modulus and defect concentration was found.[28] It is important to note that the thermal expansion behavior and the bulk modulus are fundamentally linked through the lattice dynamics and in the large picture of thermodynamics by entropy.[2] Following this thought, the post-synthetic introduction of additional connectivities between different open metal sites is intriguing and seems the natural development in the current attempts to exploit defect-engineering as tool for manipulating properties of MOFs. Only recently, Yaghi *et al.* reported that the mechanically unstable MOF-520 can be stabilized by incorporation of a rigid 4,4′-biphenyldicarboxylate (BPDC) linker as an additional connectivity to afford a mechanically robust framework. They coined the term retrofitting, describing the post-synthetic introduction of additional network connectivity into a parent MOF. When full crystallographic occupancy of the retrofitted connectivity is obtained, the defect would have been fully incorporated into the structure motif of the network; however, only 70% occupancy was observed in the bulk powder, in principle presenting a defective state of the material. Zhou *et al.* followed the same approach, reporting on the incorporation of dicarboxylate ligands in the structure of the PCN-606 family with reaching occupancies of up to 56%.[30] Having these developments in mind, it is therefore intriguing to ask '*how does retrofitting influence the NTE behavior of a MOF?*'.

Here we present a combined experimental and computational study, showing that the NTE behavior of MOFs can be tuned by retrofitting. As a model system, we focus on the MOF Cu_3BTC_2 (Figure 1a), allowing us to build on from the vast literature that exists on the host-guest chemistry in this system.[31-34] It has been established that the vacant Cu coordination sites in Cu_3BTC_2 can act as anchor points for molecules such as TCNQ. These then bridge two adjacent metal sites, creating a secondary network within Cu_3BTC_2.[35] Crystallographic evidence for the ordered arrangement of TCNQ in the bridging position has recently been found when TCNQ@Cu_3BTC_2 is prepared by TCNQ incorporation via the vapor phase.[36] The vapor phase loading of TCNQ into Cu_3BTC_2 allows for a precise control over the amount of TCNQ introduced into the framework, providing us with a tool to investigate the impact of TCNQ incorporation on the negative thermal expansion behavior. Therefore, we performed variable temperature powder X-ray diffraction (VTPXRD) experiments as well as far infrared (FIR) spectroscopy on a series of TCNQ@Cu_3BTC_2 samples. We combine our experimental results with model calculations, in which the bridging TCNQ is modelled by a harmonic spring (Figure 1b), allowing us to insight the phonon-based mechanism for the tunability of NTE behavior in this system qualitatively.

Powder samples of *x*TCNQ@Cu_3BTC_2 with *x* = 0, 0.2, 0.4, 0.6 and 1.0 were prepared by following an optimized vapor phase assisted synthesis, see experimental section below. We previously showed that this approach is superior to wet chemical infiltration techniques, enabling the preparation of samples that maintain a high residual BET surface area upon TCNQ incorporation,[36] e.g. 865.9 m²/g for 1.0TCNQ@Cu_3BTC_2 (see SI). High resolution variable temperature powder X-ray diffractograms were recorded at the Diamond Lightsource, beamline I11. Lattice parameters and volumes were extracted through a Pawley profile fit analysis within the space-group *F*m-3m. Stacking plots and statistics of all refinements are given in the SI. The volume as a function of temperature for different *x*TCNQ@Cu_3BTC_2 loadings is shown in Figure 2a. The thermal expansion coefficient α_V is extracted from the slope of the linear regression, following eq.1. The largest α_V is found for *x* = 0 with α_V = -15.3·10^{-6} K^{-1}. This value is in good agreement with literature data, where an NTE coefficient of α_V = -12.3·10^{-6} K^{-1}

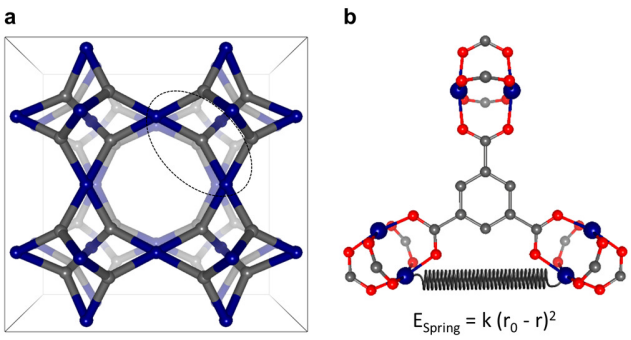

Figure 1. (a) tbo topology of Cu_3BTC_2 in which blue and grey spheres represent metal nodes and linker molecules, respectively. The dashed ellipse indicates the position of the zoom-in (b), *i.e.* three Cu paddlewheel units interconnected by BTC. Neighboring paddlewheel units can be bridged by a TCNQ molecule, which in our computational model is approximated by a mechanical spring.

has been reported for guest-free Cu_3BTC_2.[21] The slightly higher value of α_V obtained in this study likely results from a different preparation protocol, which involved very extensive solvent exchange steps and high-vacuum activation, see experimental section for details. With increasing the TCNQ loading from $x = 0.2$ to $x = 1.0$, α_V decreases monotonically to $\alpha_V = -8.4 \cdot 10^{-6}$ K^{-1} for $x = 1.0$, see Figure 2b. PTE is not observed, which is different from related studies that show a guest-dependent change from NTE to PTE.[24-25] We attribute this difference to the relatively large residual porosity at high TCNQ loadings, which seems to maintain a part of the mechanism that is responsible for NTE in Cu_3BTC_2. Therefore, TCNQ loading presents a valuable tool for fine-tuning the negative thermal expansion behavior of Cu_3BTC_2, implicating that TCNQ incorporation directly affects the underlying NTE mechanism in Cu_3BTC_2. We now turn our attention towards the origin for altered NTE.

Previously it has been shown that NTE in Cu_3BTC_2 originates from low energy collective lattice modes and local distortions of the linker and node, *i.e.* trampoline-like motions of BTC and rotor-like motions of the Cu paddlewheel moiety.[21, 37-38] In other words, increasing the temperature leads to an activation of phonon modes and vibrations that lead to a volume contraction. Staying within the quasi-harmonic approximation, it has been shown that α_V can be expressed as,[39]

$$\alpha_V(T) = 1/KV \sum_i \gamma_i C_{Vi}(T) \qquad \text{(eq. 2)}$$

with K the bulk modulus, V the volume, γ_i the Grüneisen parameter and $C_{Vi}(T)$ the isochoric specific heat. For the xTCNQ@Cu_3BTC_2 system studied here, decrease of $|\alpha_V|$ as function of unit cell volume (similarly TCNQ loading) is observed, see Figure 2b. Based on eq. 2, such a behavior first seems contradicting; however, looking at the previous finding by Yaghi *et al.* who reported a significant increase of bulk modulus in MOF-520 after retrofitting, it is reasonable assumption that any volume contributions are outweighed by a significant stiffening of the framework after TCNQ incorporation. Therefore, we ascribe the here observed decrease of $|\alpha_V|$ as a function of TCNQ loading to an allover stiffening of the Cu_3BTC_2 framework, *i.e.* an increase of bulk modulus in eq. 2. It is important to highlight at this point that the complexity behind the origin of NTE, particularly in materials with many different chemical interactions and open pore space such as MOFs, currently challenges our understanding. Therefore, it is worth mentioning that some contradicting results to eq. 2 have been reported in the past, in which a correlation between the reduction of unit cell volume and a decrease of $|\alpha_V|$ has been observed.[12, 15, 26, 40]

Whilst the reduced NTE in TCNQ@Cu_3BTC_2 is expected to have major contributions from the bulk term 1/KV in eq. 2, it is also interesting to consider the summation, which contains information about the individual modes. For instance, γ_i tells us how the frequency of a mode responds to volumes changes, with a negative change corresponding to NTE. The factor $C_{vi}(T)$ then only applies a weighting scheme, since lower frequency modes have higher thermal populations and in turn have a larger overall contribution. To gain insight into how collective modes are affected through TCNQ infiltration, we developed a heuristic spring model of the situation. In this model, TCNQ is simplified as a harmonic spring, which bridges the adjacent Cu coordination sites (see Figure 1b). Importantly, we can use this model to apply force-field based phonon calculations within the quasi-harmonic approximation and can access the change of lattice dynamics as a function of spring constant strength. In a first step, we calculated the thermal expansion coefficient of the spring-free Cu_3BTC_2 (or similarly spring strength $k = 0$ eV/Å²) to verify that the applied force field can indeed reproduce NTE behavior. Our calculations lead to $\alpha_V = -18.7 \cdot 10^{-6}$ K^{-1}, which is in reasonable agreement with our experimentally observed value. At this point, we want to emphasize that the applied computationally methodology is not set up to reproduce experimental results but to investigate the impact of TCNQ incorporation on the lattice dynamics qualitatively. In a second step, we then gradually increased the force constant between $k = 0 - 7$ eV/Å², see Figure 3a. Analogous to our experiments we observe that $|\alpha_V|$ and K increase as a function of spring constant. This finding supports our previous speculation that the reduction of NTE in TCNQ@Cu_3BTC_3 is mainly driven by a stiffening of the framework, i.e. an increase of K as a function of TNCQ loading. Interestingly, α_V remains negative for all spring constants, revealing that the sum in eq.2 remains negative despite the presence of the spring. To investigate the impact of the spring on the phonon modes in more detail, we calculated the difference of frequencies $\Delta\omega = \omega_0 - \omega_7$ at $k = 7$ and 0 eV/Å², see Figure 3b. A mode stiffening in the low energy region can be observed whilst modes at higher frequencies show a small or vanishing change in energy. We also observe some changes in the mode-Grüneisen parameters as a function of ω; however, the allover summation from eq. 2 remains negative and a negative sign of α_V is mainained. With these results on hand, we performed FIR spectroscopy to probe if any evidence for mode changes as a function of TCNQ incorporation become evident. It should be pointed out, however, that IR only probes phonon dynamics at wave vectors close to 0. Moreover, only phonon changes related to optic modes are accessible due to selection rules of the method; however, previously it has been shown that optic modes can have an impact on the NTE behavior in MOFs;

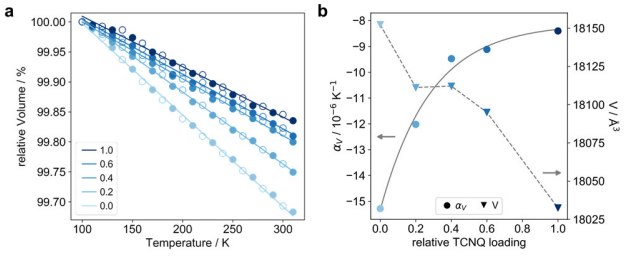

Figure 2. (a) Relative unit cell volume of xTCNQ@Cu_3BTC_2 (x given in the legend) plotted against the temperature. Data from cooling (empty circles) and heating (filled circles) cycle was recorded in 20 K steps. (b) Thermal expansion coefficient (α_V) and unit cell volume (V, at 100 K) of xTCNQ@Cu_3BTC_2 plotted against the relative TCNQ loading. The solid and dashed lines are a guide to the eyes.

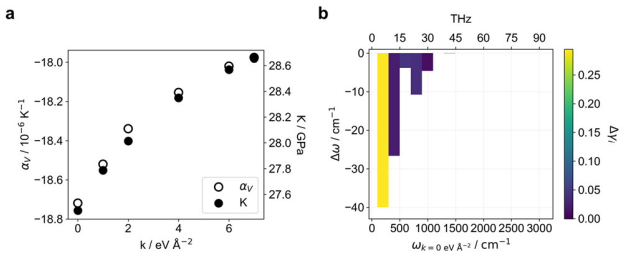

Figure 3. (a) Calculated thermal expansion coefficient α_V and bulk modulus K with variation of the spring constant k between neighboring Cu paddlewheel moieties. (b) Difference in mode frequencies between k = 0 and k = 7 evA^{-2}, with a negative value of $\Delta\omega$ indicating a stiffening of the mode and in turn a decrease in the thermal expansion coefficient α_V.

for instance, the abovementioned bending mode of the benzendicarboxylate linker in MOF-5 represents such a mode.[20, 22-23] Indeed, we observe several FIR bands in the low frequency region that show an increase of frequency as a function of TCNQ loading, see Figure 4. The largest blue shift is observed for the band at 40.0 cm^{-1} in Cu_3BTC_2 increasing by 7.9 cm^{-1} in the sample with x = 1.0. For bands at higher frequencies, however, we observe the opposite trend (see SI) showing a shift to lower frequencies, generally supporting the results from our calculations.

In conclusion we have shown that the post-synthetic incorporation of additional connectivity into a MOF – retrofitting – is a suitable approach to control the thermal expansion behavior. As prototypical example, we studied the incorporation of TCNQ into Cu_3BTC_2, a host-guest system that caused some excitement in the context of electrically conductive MOFs. We show that NTE in Cu_3BTC_3 can be controlled as a function of TCNQ loading, an effect that is ascribed to a stiffening of the material. Our heuristic computational model shows, however, that a certain mode stiffening occurs at the same time, emphasizing the interrelation of the complex parameters that determine the magnitude as well as the sign of thermal expansion behavior in MOFs.

At this point, a couple of things are important to mention. Firstly, it should be noted that examples of retrofitted MOFs were known before retrofitting as concept has been proposed in 2017;[35, 41-44] however, retrofitting per sé is a useful categorization that describes a distinct approach to post-synthetically modify MOFs. Moreover, based on our results it seems that retrofitting is a universal approach to access materials properties, which in principle can be applied to all MOFs with open metal sites or more generally, functional groups and sites. Conceptually, retrofitting of MOFs leads to a defective state, when the incorporated guest exhibits only partial occupancy. It will be interesting so see if in the future full occupancy can be achieved, thereby leaving the territory of a defective state. Furthermore, it should be emphasized that such an introduction of defects is inherently absent in non-porous materials, highlighting the opportunities experimentalists have in manipulating materials properties of MOFs.

Experimental Section

Synthesis: Cu_3BTC_2 samples with different loadings of TCNQ were synthesized following an optimized vapor phase infiltration procedure[36] using high-vacuum glass ampules to enhance the sublimation and diffusion of TCNQ. Stoichiometric amounts of TCNQ were thoroughly mixed with activated Cu_3BTC_2 (100 mg) and filled into high-vacuum glass ampules, which were then evacuated to 10^{-5} mbar and flame sealed. The ampules were placed in a convection oven at 180 °C for 72 h to yield a series of xTCNQ@Cu_3BTC_2 with x = n(TCNQ)/n(Cu_3BTC_2) = 0.2, 0.4, …, 1.0. Activated and TCNQ-loaded samples were handled under argon at all times to avoid adsorption of water which would compromise the obtained results. All measurements were performed under inert conditions.

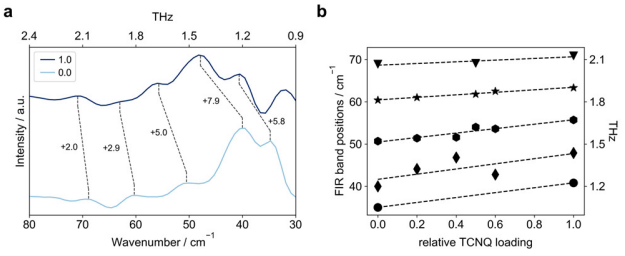

Figure 4. (a) Low frequency FIR spectra of Cu_3BTC_2 (light blue) and 1.0TCNQ@Cu_3BTC_2 (dark blue). The spectra are normalized, and a vertical offset is applied for clarity. (b) Shift of FIR band positions with TCNQ loading. All corresponding FIR spectra are provided in the SI.

VTPXRD: High-resolution variable temperature powder X-ray diffraction was performed at beamline I11 of the Diamond Lightsource in transmission geometry. Therefore, the samples were filled into 0.5 mm quartz capillaries inside an Ar-filled glovebox and sealed using two-component adhesive. The operating wavelength was λ = 0.824945(10) Å and the photosensitive detector was used for data collection. Temperature control was applied by using an Oxford Cryosystem, in which the samples were first cooled down from RT to 100 K in 20 K steps before the temperature was increased from 110 K to 310 K. Before every measurement, the temperature was allowed to stabilize for 120 s. Quantitative data analysis, *i.e.* Pawley profile fits to extract lattice parameters were performed by using TOPAS academic v5.

Far-infrared spectroscopy: Far infrared spectra were recorded on a Bruker VERTEX 70V vacuum spectrometer in the range of 600 – 30 cm^{-1}. The instrument was equipped with a Si-supported beamsplitter, a ceramic source and a DTGS detector using a GladiATR accessory (Pike, USA).

Calculations: Thermal expansion coefficients were calculated in a quasi-harmonic approach using the force-field code GULP[45] with the UFF4MOF library[46] by applying cell parameter deviations of ±0.5% in 0.1% steps. In all calculations, a free-energy optimizer was used in the approximation of only considering the first 100 modes at the Gamma point. Mode-Grüneisen parameters were calculated from the frequency and volume changes of the maximum expansion and contraction and equilibrium structure.

ASSOCIATED CONTENT

Supporting Information. Further information about the synthesis, porosimetry measurements, VTPXRD measurements and vibrational spectroscopy is provided in the SI. This material is available free of charge via the Internet at http://pubs.acs.org.

AUTHOR INFORMATION

Corresponding Author

* Department of Chemistry, Technical University Munich, Lichtenbergstrasse 4, D-85748 Garching, Germany.
E-Mail: gregor.kieslich@tum.de

Author Contributions

The manuscript was written through contributions of all authors. All authors have given approval to the final version of the manuscript.

Funding Sources

DFG SPP1928 (COORNETs)

ACKNOWLEDGMENT

We like to thank Chiu Tang for support during data collection at beam line I11 at the Diamond Light Source (EE17914). CS acknowledges his scholarships from the Studienstiftung des Deutschen Volkes and from the Fonds der Chemischen Industrie. GK gratefully thanks the Fonds der Chemischen Industrie and the DFG SPP1928 (COORNETs) for financial support.

REFERENCES

1. Miller, W.; Smith, C. W.; Mackenzie, D. S.; Evans, K. E., Negative Thermal Expansion: A Review. *J. Mater. Sci.* **2009,** *44*, 5441-5451.
2. Dove, M. T.; Fang, H., Negative Thermal Expansion and Associated Anomalous Physical Properties: Review of the Lattice Dynamics Theoretical Foundation. *Rep. Prog. Phys.* **2016,** *79*, 066503.
3. Coates, C. S.; Goodwin, A. L., How to Quantify Isotropic Negative Thermal Expansion: Magnitude, Range, or Both? *Mater Horiz.* **2019**.
4. Li, W.; Probert, M. R.; Kosa, M.; Bennett, T. D.; Thirumurugan, A.; Burwood, R. P.; Parinello, M.; Howard, J. A. K.; Cheetham, A. K., Negative Linear Compressibility of a Metal–Organic Framework. *J. Am. Chem. Soc.* **2012,** *134*, 11940-11943.
5. Cairns, A. B.; Catafesta, J.; Levelut, C.; Rouquette, J.; van der Lee, A.; Peters, L.; Thompson, A. L.; Dmitriev, V.; Haines, J.; Goodwin, A. L., Giant Negative Linear Compressibility in Zinc Dicyanoaurate. *Nat. Mater.* **2013,** *12*, 212.
6. Baughman, R. H.; Stafström, S.; Cui, C.; Dantas, S. O., Materials with Negative Compressibilities in One or More Dimensions. *Science* **1998,** *279*, 1522-1524.
7. Huang, C.; Chen, L., Negative Poisson's Ratio in Modern Functional Materials. *Adv. Mater.* **2016,** *28*, 8079-8096.
8. Rothenburg, L.; Ai. Berlin, A. I.; Bathurst, R. J., Microstructure of Isotropic Materials with Negative Poisson's Ratio. *Nature* **1991,** *354*, 470-472.
9. Lakes, R., Foam Structures with a Negative Poisson's Ratio. *Science* **1987,** *235*, 1038-1040.
10. Martinek, C.; Hummel, F. A., Linear Thermal Expansion of Three Tungstates. *J. Am. Ceram. Soc.* **1968,** *51*, 227-228.
11. S. O. Evans, J., Negative Thermal Expansion Materials *Dalton Trans.* **1999**, 3317-3326.
12. Goodwin, A. L.; Kepert, C. J., Negative Thermal Expansion and Low-Frequency Modes in Cyanide-Bridged Framework Materials. *Phys. Rev. B* **2005,** *71*, 140301.
13. Goodwin, A. L.; Kennedy, B. J.; Kepert, C. J., Thermal Expansion Matching via Framework Flexibility in Zinc Dicyanometallates. *J. Am. Chem. Soc.* **2009,** *131*, 6334-6335.
14. Attfield, M. P.; Sleight, A. W., Exceptional Negative Thermal Expansion in AlPO4-17. *Chem. Mater.* **1998,** *10*, 2013-2019.
15. Lightfoot, P.; Woodcock, D. A.; Maple, M. J.; Villaescusa, L. A.; Wright, P. A., The Widespread Occurrence of Negative Thermal Expansion in Zeolites. *J. Mater. Chem.* **2001,** *11*, 212-216.
16. Chen, J.; Gao, Q.; Sanson, A.; Jiang, X.; Huang, Q.; Carnera, A.; Rodriguez, C. G.; Olivi, L.; Wang, L.; Hu, L.; Lin, K.; Ren, Y.; Lin, Z.; Wang, C.; Gu, L.; Deng, J.; Attfield, J. P.; Xing, X., Tunable Thermal Expansion in Framework Materials Through Redox Intercalation. *Nat. Commun.* **2017,** *8*, 14441.
17. Tranchemontagne, D. J.; Mendoza-Cortes, J. L.; O'Keeffe, M.; Yaghi, O. M., Secondary Building Units, Nets and Bonding in the Chemistry of Metal-Organic Frameworks. *Chem. Soc. Rev.* **2009,** *38*, 1257-1283.
18. Kitagawa, S.; Kitaura, R.; Noro, S.-i., Functional porous coordination polymers. *Angew. Chem., Int. Ed.* **2004,** *43*, 2334-2375.
19. Lock, N.; Christensen, M.; Wu, Y.; Peterson, V. K.; Thomsen, M. K.; Piltz, R. O.; Ramirez-Cuesta, A. J.; McIntyre, G. J.; Norén, K.; Kutteh, R.; Kepert, C. J.; Kearley, G. J.; Iversen, B. B., Scrutinizing Negative Thermal Expansion in MOF-5 by Scattering Techniques and Ab Initio Calculations. *Dalton Trans.* **2013,** *42*, 1996-2007.
20. Lock, N.; Wu, Y.; Christensen, M.; Cameron, L. J.; Peterson, V. K.; Bridgeman, A. J.; Kepert, C. J.; Iversen, B. B., Elucidating Negative Thermal Expansion in MOF-5. *J. Phys. Chem. C* **2010,** *114*, 16181-16186.
21. Wu, Y.; Kobayashi, A.; Halder, G. J.; Peterson, V. K.; Chapman, K. W.; Lock, N.; Southon, P. D.; Kepert, C. J., Negative Thermal Expansion in the Metal–Organic Framework Material Cu3(1,3,5-benzenetricarboxylate)2. *Angew. Chem. Int. Ed.* **2008,** *47*, 8929-8932.
22. Zhou, W.; Wu, H.; Yildirim, T.; Simpson, J. R.; Walker, A. H., Origin of the Exceptional Negative Thermal Expansion in Metal-Organic Framework-5 Zn4O(1, 4−Benzenedicarboxylate)3. *Phys. Rev. B* **2008,** *78*, 054114.
23. Rimmer, L. H. N.; Dove, M. T.; Goodwin, A. L.; Palmer, D. C., Acoustic Phonons and Negative Thermal Expansion in MOF-5. *Phys. Chem. Chem. Phys.* **2014,** *16*, 21144-21152.
24. Lock, N.; Christensen, M.; Kepert, C. J.; Iversen, B. B., Effect of Gas Pressure on Negative Thermal Expansion in MOF-5. *Chem. Commun.* **2013,** *49*, 789-791.
25. Balestra, S. R. G.; Bueno-Perez, R.; Hamad, S.; Dubbeldam, D.; Ruiz-Salvador, A. R.; Calero, S., Controlling Thermal Expansion: A Metal–Organic Frameworks Route. *Chem. Mater.* **2016,** *28*, 8296-8304.
26. Cliffe, M. J.; Hill, J. A.; Murray, C. A.; Coudert, F.-X.; Goodwin, A. L., Defect-Dependent Colossal Negative Thermal Expansion in UiO-66(Hf) Metal–Organic Framework. *Phys. Chem. Chem. Phys.* **2015,** *17*, 11586-11592.
27. Dissegna, S.; Epp, K.; Heinz, W. R.; Kieslich, G.; Fischer, R. A., Defective Metal-Organic Frameworks. *Adv. Mater.* **2018,** *30*.
28. Dissegna, S.; Vervoorts, P.; Hobday, C. L.; Düren, T.; Daisenberger, D.; Smith, A. J.; Fischer, R. A.; Kieslich, G., Tuning the Mechanical Response of Metal–Organic Frameworks by Defect Engineering. *J. Am. Chem. Soc.* **2018,** *140*, 11581-11584.
29. Kapustin, E. A.; Lee, S.; Alshammari, A. S.; Yaghi, O. M., Molecular Retrofitting Adapts a Metal–Organic Framework to Extreme Pressure. *ACS Cent. Sci.* **2017,** *3*, 662-667.
30. Lollar, C. T.; Pang, J.; Qin, J.-s.; Yuan, S.; Powell, J. A.; Zhou, H.-C., Thermodynamically Controlled Linker Installation in Flexible Zirconium Metal–Organic Frameworks. *Cryst. Growth Des.* **2019**.
31. Prestipino, C.; Regli, L.; Vitillo, J. G.; Bonino, F.; Damin, A.; Lamberti, C.; Zecchina, A.; Solari, P.; Kongshaug, K.; Bordiga, S., Local Structure of Framework Cu (II) in HKUST-1 Metallorganic Framework: Spectroscopic Characterization upon Activation and Interaction with Adsorbates. *Chem. Mater.* **2006,** *18*, 1337-1346.
32. Allendorf, M. D.; Foster, M. E.; Léonard, F.; Stavila, V.; Feng, P. L.; Doty, F. P.; Leong, K.; Ma, E. Y.; Johnston, S. R.; Talin, A. A., Guest-Induced Emergent Properties in Metal–Organic Frameworks. *J. Phys. Chem. Lett.* **2015,** *6*, 1182-1195.
33. Hendon, C. H.; Walsh, A., Chemical Principles Underpinning the Performance of The Metal-Organic Framework HKUST-1. *Chem. Sci.* **2015,** *6*, 3674-3683.
34. Souza, B. E.; Rudić, S.; Titov, K.; Babal, A. S.; Taylor, J. D.; Tan, J.-C., Guest–Host Interactions of Nanoconfined Anti-Cancer Drug in Metal–Organic Framework Exposed by Terahertz Dynamics. *Chem. Commun.* **2019**.
35. Talin, A. A.; Centrone, A.; Ford, A. C.; Foster, M. E.; Stavila, V.; Haney, P.; Kinney, R. A.; Szalai, V.; El Gabaly, F.; Yoon, H. P.; Léonard, F.; Allendorf, M. D., Tunable Electrical Conductivity in Metal-Organic Framework Thin-Film Devices. *Science* **2014,** *343*, 66-69.
36. Schneider, C.; Ukaj, D.; Koerver, R.; Talin, A. A.; Kieslich, G.; Pujari, S. P.; Zuilhof, H.; Janek, J.; Allendorf, M. D.; Fischer, R. A., High Electrical Conductivity and High Porosity in a Guest@MOF Material: Evidence of TCNQ Ordering within Cu3BTC2 Micropores. *Chem. Sci.* **2018,** *9*, 7405-7412.
37. Peterson, V. K.; Kearley, G. J.; Wu, Y.; Ramirez-Cuesta, A. J.; Kemner, E.; Kepert, C. J., Local Vibrational Mechanism for Negative Thermal Expansion: A Combined Neutron Scattering and First-Principles Study. *Angew. Chem. Int. Ed.* **2010,** *49*, 585-588.
38. Ryder, M. R.; Civalleri, B.; Cinque, G.; Tan, J.-C., Discovering Connections between Terahertz Vibrations and Elasticity Underpinning the Collective Dynamics of the HKUST-1 Metal–Organic Framework. *CrystEngComm* **2016,** *18*, 4303-4312.
39. Wang, K.; Reeber, R. R., Mode Grüneisen Parameters and negative Thermal Expansion of Cubic ZrW2O8 and ZrMo2O8. *Appl. Phys. Lett.* **2000,** *76*, 2203-2204.
40. Chapman, K. W.; Chupas, P. J.; Kepert, C. J., Compositional Dependence of Negative Thermal Expansion in the Prussian Blue

Analogues MIIPtIV(CN)6 (M = Mn, Fe, Co, Ni, Cu, Zn, Cd). *J. Am. Chem. Soc.* **2006,** *128*, 7009-7014.

41. Chen, C. X.; Wei, Z.; Jiang, J. J.; Fan, Y. Z.; Zheng, S. P.; Cao, C. C.; Li, Y. H.; Fenske, D.; Su, C. Y., Precise Modulation of the Breathing Behavior and Pore Surface in Zr-MOFs by Reversible Post-Synthetic Variable-Spacer Installation to Fine-Tune the Expansion Magnitude and Sorption Properties. *Angew. Chem. Int. Ed.* **2016,** *55*, 9932-9936.

42. Chen, C.-X.; Wei, Z.-W.; Jiang, J.-J.; Zheng, S.-P.; Wang, H.-P.; Qiu, Q.-F.; Cao, C.-C.; Fenske, D.; Su, C.-Y., Dynamic Spacer Installation for Multirole Metal–Organic Frameworks: A New Direction toward Multifunctional MOFs Achieving Ultrahigh Methane Storage Working Capacity. *J. Am. Chem. Soc.* **2017,** *139*, 6034-6037.

43. Wang, T. C.; Hod, I.; Audu, C. O.; Vermeulen, N. A.; Nguyen, S. T.; Farha, O. K.; Hupp, J. T., Rendering High Surface Area, Mesoporous Metal–Organic Frameworks Electronically Conductive. *ACS Appl. Mater. Interfaces* **2017,** *9*, 12584-12591.

44. Yuan, S.; Lu, W.; Chen, Y.-P.; Zhang, Q.; Liu, T.-F.; Feng, D.; Wang, X.; Qin, J.; Zhou, H.-C., Sequential Linker Installation: Precise Placement of Functional Groups in Multivariate Metal–Organic Frameworks. *J. Am. Chem. Soc.* **2015,** *137*, 3177-3180.

45. Gale, J. D.; Rohl, A. L., The General Utility Lattice Program (GULP). *Mol. Simulat.* **2003,** *29*, 291-341.

46. Addicoat, M. A.; Vankova, N.; Akter, I. F.; Heine, T., Extension of the Universal Force Field to Metal–Organic Frameworks. *J. Chem. Theory Comput.* **2014,** *10*, 880-891.